The effect of compressibility on vortex pairing

N. D. Sandham
Department of Aeronautical Engineering, Queen Mary and Westfield College, Mile End Road, London E1 4NS, England

(Received 12 March 1993; accepted 26 October 1993)

Direct numerical simulations are conducted to investigate in detail the effect of Mach number on vortex pairing in a mixing layer. The pairing process is found to be delayed at higher Mach numbers and the paths followed by the vortices change. To investigate the effect of the initial shape of the vortices a simple vortex dynamical model of pairing is constructed which accurately models pairing at low Mach numbers. Results from the model suggest that a variation in the initial shape of the vortices is not sufficient to explain the changes in the pairing process due to Mach number. Further simulations are conducted for isolated vortex pairs. There is little departure from the expected rotation rate as Mach number is increased, but strong core effects. Overall, changes in the pairing process reflect changes in the evolution of the primary instability, with vortex trajectories becoming more elongated as the Mach number is increased.

I. INTRODUCTION

Compressibility can have strong effects on shear layers, the most well known being the reduction in growth rate of the mixing layer. At Mach numbers where the mixing layer growth rate is less than a half of its incompressible value both flow visualizations and numerical simulations show turbulent flow with eddying motions. Interpretation of the results from such studies in terms of vortex motions is difficult since the subject of vortex dynamics is based almost exclusively on incompressible flow (an exception is the work of Moore[1]). It is therefore important to learn as much as possible about the effect of compressibility on elementary vortex interactions, so that for a given flow, where the flow structure or dominant mechanism is known from incompressible work, the primary effects of compressibility can be predicted.

The reduction in growth rate of the mixing layer as Mach number is increased matches the decrease in the growth rate of small disturbances, as obtained by linear stability theory. Figure 1 shows a typical plot from linear stability theory (in this case temporal theory). The maximum value of the growth rate for waves of any orientation is shown. The most unstable wave is two dimensional up to a convective Mach number of 0.6 and thereafter oblique with increasing angle. Sandham and Reynolds[2,3] carried out two- and three-dimensional simulations of the mixing layer. These showed that the two-dimensional (2-D) structures resulting from the nonlinear evolution of the linear eigenfunctions became more elongated as the Mach number was increased. Above a convective Mach number of 0.6 it was confirmed that the organized structure in the mixing layer changed from being dominated by spanwise vortices, to a much more three-dimensional (3-D) structure. The change has also been found in the experiments of Clemens and Mungal.[4] In the simulations a double-Λ structure was proposed for the mixing layer at convective Mach numbers above unity.

Although earlier work concentrated on the three-dimensional effects at high Mach number, it is clear that many of the fundamental effects of compressibility appear at much lower Mach numbers and deserve more detailed study. From Fig. 1 it can be seen that half the reduction in growth rate occurs before a convective Mach number of 0.6. In some of the earlier work using two-dimensional simulations of the compressible Navier–Stokes equations Sandham and Reynolds[2] observed changes in the vortex pairing process. Three alternative possibilities were then offered to explain this:

(a) That the change in the shape of the original vortices that formed from the instability of the flow was responsible;

(b) that the rate of rotation of the vortices around each other was affected by compressibility;

(c) that the compressibility effects that led to the reduced linear instability of the mixing layer continued to operate during the pairing process.

In this paper further investigations are made into the mechanisms affecting the pairing process as Mach number is increased. First, in Sec. II, a series of direct numerical simulations are presented, and detailed data concerning the pairing process is extracted. In Sec. III, the question of vortex shape is addressed. A model of the pairing process based on a simple vortex sheet representation of the pairing vortices is developed and tested. In Sec. IV simulations of isolated corotating vortices are made. Conclusions are then drawn as to the most likely causes of the compressibility effects.

II. DIRECT NUMERICAL SIMULATIONS OF VORTEX PAIRING

A series of simulations of vortex merging in a mixing layer have been made. To complement previous simulations[2] these were made using a fixed computational box length and a fixed initial disturbance. This removed some of the variables from the earlier simulations, where the eigenfunctions from inviscid linear stability theory were used and the box length was fixed by twice the wavelength of the most unstable wave. In the earlier simulations

 1070-6631/94/6(2)/1063/10/$6.00

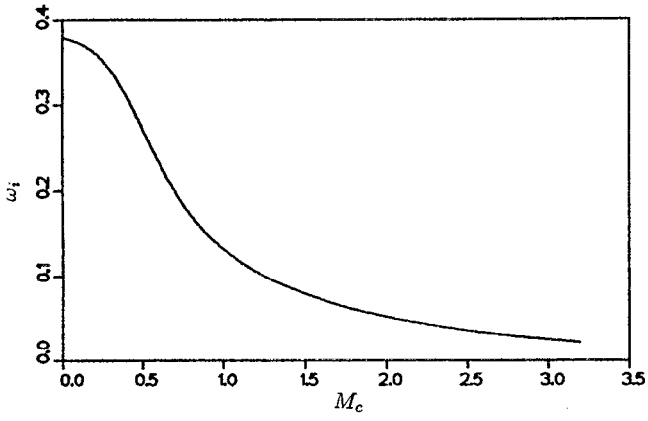

FIG. 1. Growth rate ω_i of small disturbances in the mixing layer, as a function of convective Mach number (from temporal inviscid linear stability theory).

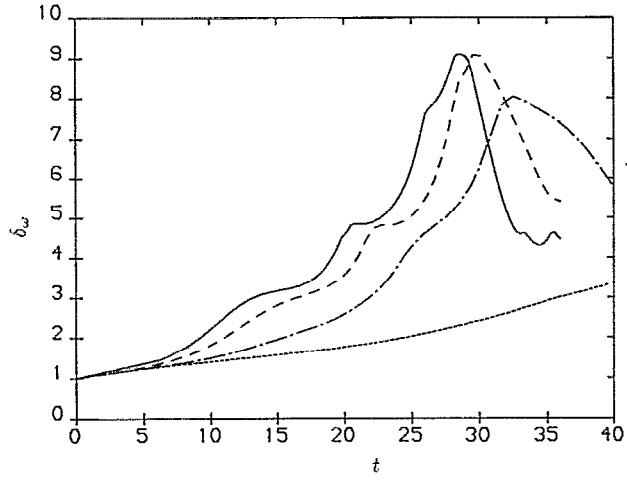

FIG. 2. Variation of vorticity thickness with time for $M_c=0.2$(——), 0.4(– – –), 0.6(– – –), and 0.8(----).

it was not always clear whether an effect stemmed from the intrinsic compressibility of the flow, or from box length effects.

The simulations were made for a temporally evolving mixing layer with equal and opposite free-stream velocities and equal free-stream densities. Lengths are normalized by the initial vorticity thickness (the ratio of the velocity difference between the two free streams to the maximum gradient of the average velocity profile) and velocities by the magnitude of the free-stream velocity. The nondimensionalized initial velocity profile is given by

$$\bar{u}=\tanh(2y), \tag{1}$$

and the nondimensionalized initial temperature profile by the Crocco–Busemann relation

$$\bar{T}=1+\frac{\gamma-1}{2}M_c^2(1-\bar{u}^2), \tag{2}$$

where M_c is the convective Mach number of the flow. For this case $M_c=U_1/a_1$, where U_1 is the free-stream velocity and a_1 is the free-stream sound speed. Pressure is assumed to be uniform, allowing a nondimensional density to be calculated as the inverse of the temperature.

To force the pairing process, disturbances were added to the initial mean velocity profiles. These consisted of a fundamental and a subharmonic disturbance added to form disturbances u' and v' as follows:

$$\begin{aligned} u' &= -A_1\frac{yL_x}{2\pi B}\cos\left(\frac{4\pi x}{L_x}\right)\exp\left(\frac{-y^2}{B}\right) \\ &\quad -A_2\frac{yL_x}{\pi B}\cos\left(\frac{2\pi x}{L_x}\right)\exp\left(\frac{-y^2}{B}\right), \\ v' &= A_1\sin\left(\frac{4\pi x}{L_x}\right)\exp\left(\frac{-y^2}{B}\right)+A_2\sin\left(\frac{2\pi x}{L_x}\right)\exp\left(\frac{-y^2}{B}\right). \end{aligned} \tag{3}$$

This provides a standard divergence-free disturbance to the mixing layer, with a phase of zero between the fundamental and subharmonic such that the pairing is excited most efficiently. In all the simulations the amplitudes were chosen to be $A_1=0.05$ and $A_2=0.025$. The parameter B governing the decay of the disturbance in the free stream was set equal to 10. The computational box lengths were prescribed by $L_x=20$ and $L_y=20$. Thus the wave number of the fundamental and its subharmonic are given by 0.628 and 0.314, respectively. Corresponding amplification rates ω_i are (0.338, 0.228) at $M_c=0.2$, (0.297, 0.204) at $M_c=0.4$, (0.233, 0.169) at $M_c=0.6$, and (0.139, 0.126) at $M_c=0.8$.

The simulations were made for a Reynolds number of 200 based on the initial vorticity thickness and U_1, a Prandtl number of 1, and convective Mach numbers of 0.2, 0.4, 0.6, and 0.8. The viscosity varied with temperature according to a power law with exponent 0.67. Details of the numerical method (Fourier in x and Padé in y) can be found in Sandham and Reynolds,[2] along with results from earlier simulations. In the simulations presented here 128 points were used in the x direction and 151 in the y direction. This is sufficient to fully resolve the physical phenomena and further mesh refinement would not affect the results.

An overall picture of the shear layer evolution is shown on Figs. 2 and 3. Figure 2 shows the variation of the vorticity thickness with time for a range of Mach numbers. Compressibility effects are apparent, even in the change from $M_c=0.2$ to $M_c=0.4$. By $M_c=0.8$ the shear layer growth is (at least in these two-dimensional simulations) strongly retarded. These general features are also observed when different measures of thickness, such as the momentum thickness, are used. Also, almost identical results were obtained for simulations beginning from a shear layer with a uniform mean density, indicating that the profile given by (2) is not critical. Selected views of the vorticity field during the pairing process are shown on Fig. 3 for $M_c=0.2$ and for $M_c=0.6$. Considering first the sequence for the lower Mach number, it is possible to relate the peaks and valleys of the vorticity thickness plot to events in the flow. The plateau for $14<t<17$ corresponds to saturation of the primary instability. The sharp change at $t=20$ corresponds

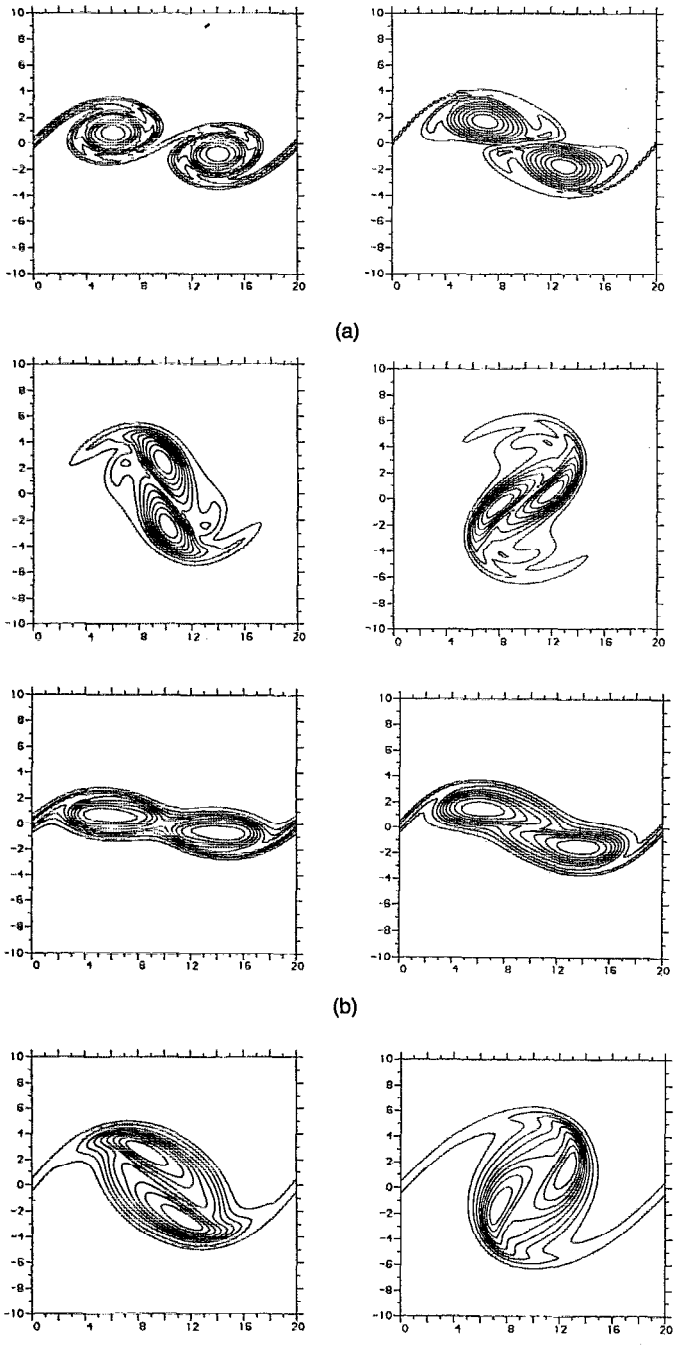

FIG. 3. Time sequence of the vorticity field in the mixing layer: (a) $M_c=0.2$ at times 18, 22.5, 27, and 31.5; (b) $M_c=0.6$ at times 21.67, 26.67, 31.67, and 36.67.

to the point at which two inflection points form in the mean velocity profile and the point for calculation of the vorticity thickness changes. This occurs at an angle of vortex rotation of approximately $\theta=20°$. The point of maximum vorticity thickness occurs at $\theta=90°$, and thereafter the vorticity thickness drops steeply. Comparison with the $M_c=0.6$ case shows how much more elongated the vortices are that form from the primary instability. Rotation proceeds generally in a similar manner to the lower Mach number case, though the details are different. The rate of decrease in vorticity thickness following the peak is slower

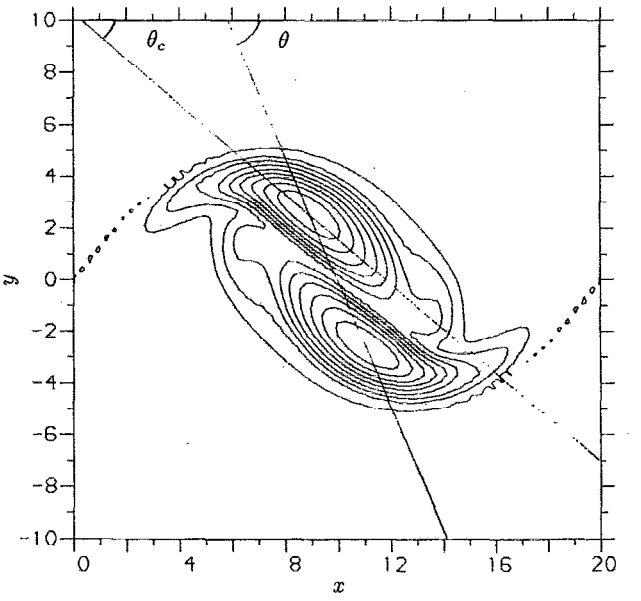

FIG. 4. Definition of d, θ, and θ_c for pairing vortices. (Plot taken from $t=28$ at $M_c=0.4$.)

at the higher Mach number. From the vorticity thickness plot it appears that a part of the increase in the time taken to reach the maximum thickness (and hence the reduced growth rate) can be attributed to the initial time delay in forming the first vortex.

To investigate in detail the pairing process more information is extracted from the time histories of the vorticity field. The spacing d and the rotation angle θ of the vortices are readily obtained. Also the angle of inclination of the cores of the vortices θ_c can be found. During the pairing the vortices are quite elongated, even at the lower Mach numbers, and so the principal axis is fairly well defined, though not as definite as the other two measures. An example of the extraction of information from the vorticity field is shown in Fig. 4. The results of this procedure are shown in Fig. 5. The normalized spacing of the vortices (equal to 1 before the pairing process) is shown in Fig. 5(a). The initial slope becomes flatter as the Mach number increases, reflecting the increased stabilization of the 2-D subharmonic secondary instability with increasing Mach numbers (Ragab and Wu[5]). The whole form of the variation of vortex spacing changes as the Mach number increases. A much more oscillatory variation is found at $M_c=0.6$, contrasting with the monotonic (up to $t=35$) decrease in vortex spacing at $M_c=0.2$. Spacing can be related to rotation by comparison with Fig. 5(b). At $M_c=0.2$ an almost linear change in angle with time is obtained, while at $M_c=0.6$ the angle shows regions of rapid change and regions of very slow movement. The angle of inclination is shown in Fig. 5(c) and by comparison with the other plots it is evident that the principal axis of the vortices rotates by 180° for 360° of vortex rotation.

Part of the effect of compressibility is the time delay due to stabilization of the flow. To isolate pairing effects Fig. 6 shows the vortex spacing and inclination plotted

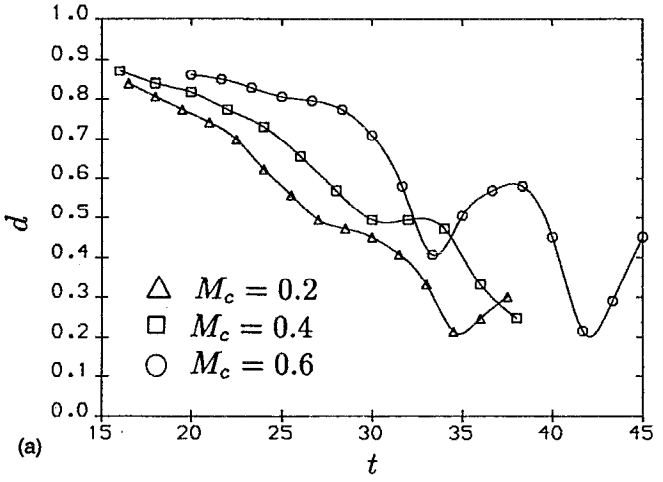

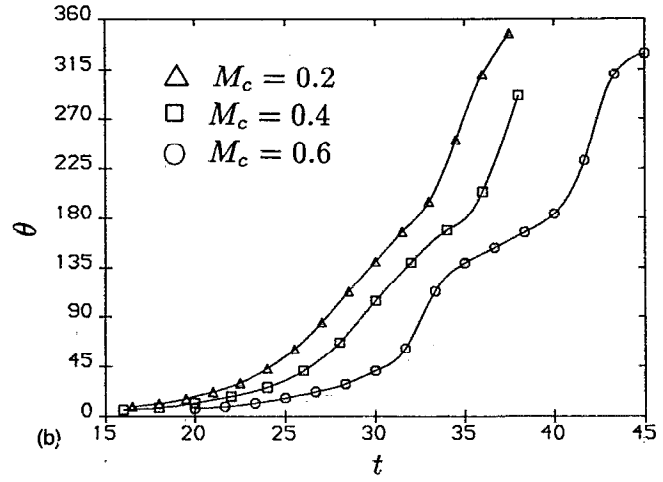

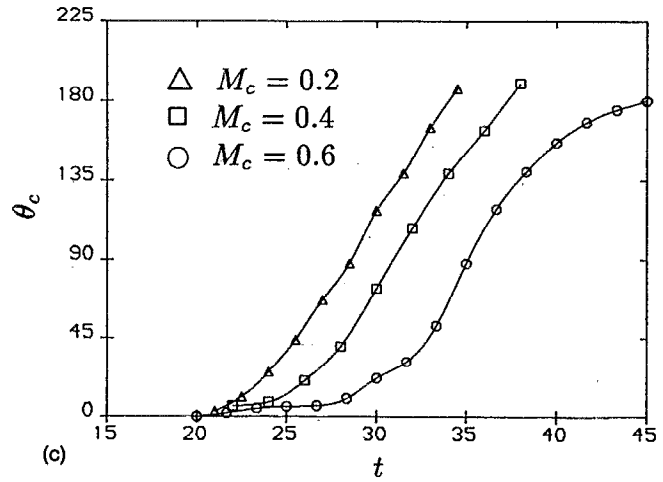

FIG. 5. Variation during pairing of (a) vortex spacing, (b) angle of rotation, and (c) angle of core inclination.

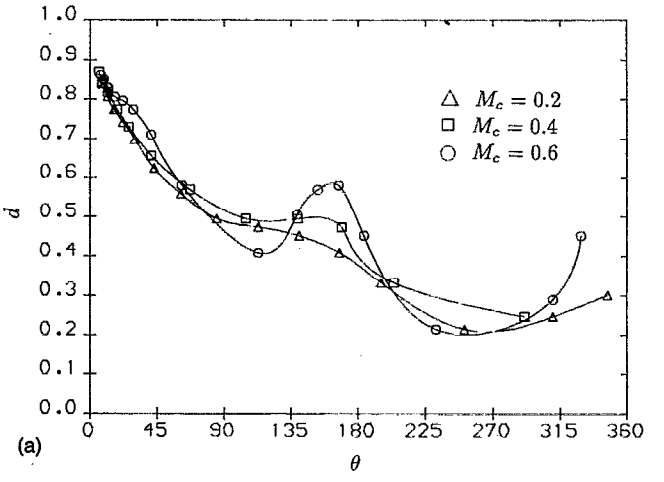

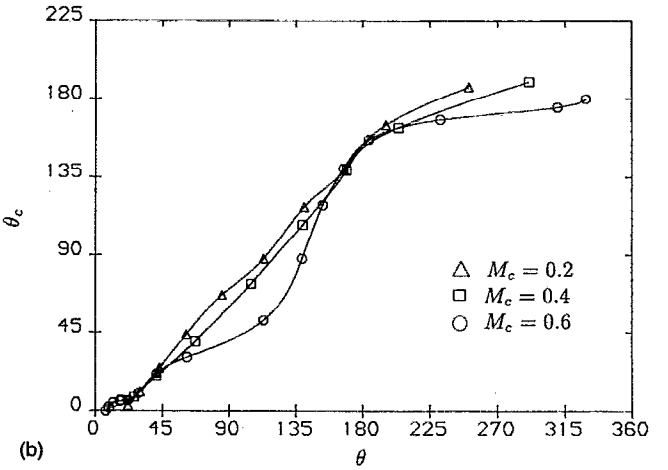

FIG. 6. Plots of the variation of (a) vortex spacing, and (b) angle of core inclination with angle of rotation.

against θ. This shows much more clearly the change in the form of the pairing process. The variation of the vortex spacing in Fig. 6(a) becomes more oscillatory as Mach number increases, with regions where the spacing actually increases. Figure 6(b) shows that the inclination angle of the cores of the vortices becomes almost constant for $45° < \theta < 110°$ at $M_c = 0.6$, before increasing rapidly up to 160° at $\theta = 180°$.

From Figs. 5 and 6 it is possible to extract a simplified picture of the change in vortex orientation during the pairing process. This is shown in Fig. 7 for the low Mach number situation, with the vortices represented by short lines aligned with the principal axes at the inclination angle θ_c to the horizontal. Initially the vortices lie at $\theta_c = 0°$. As the pairing process starts the vortices move toward each other and rotate in a clockwise sense. The axis of the vortices also rotates clockwise reaching $\theta_c = 30°$ at $\theta = 45°$ and $\theta_c = 65°$ at $\theta = 90°$. By $\theta = 90°$ the spacing of the vortices is about 50% of its original value. The rate of decrease of spacing slows as θ increases to 180°, although θ_c continues to vary, reaching 155° by $\theta = 180°$. The angular velocity of the rotation increases for $\theta > 180°$ and θ reaches 360° in another six time units, by which time the spacing has decreased to about 30% of the original and the angle of inclination remains at around 180°. This schematic picture

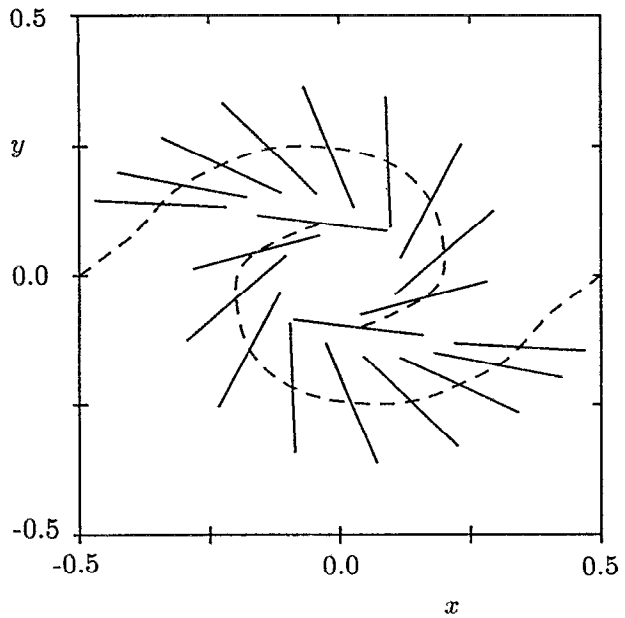

FIG. 7. Time sequence of the pairing process at low Mach number, representing the vortices by lines along the principal axis. Times vary from 21 to 34.5 in steps of 1.5. The dashed lines show the trajectories of the vortex centers. Distances are normalized by the initial vortex spacing.

of the pairing forms the basis for the investigation of shape effects in the next section.

III. EFFECT OF VORTEX SHAPE

The simplest model of the pairing process is to consider a line of point vortices. The vortices rotate around each other up to the point $\theta=90°$, moving closer together in the process. However, as the rotation proceeds the vortices move farther apart and end up at $\theta=180°$ with their original separation, having only swapped places with their neighboring vortex. The problem with this model is evidently the symmetry in the arrangement at $\theta=90°$. Models with a fixed axisymmetric core structure would all possess the same defect.

The mechanism for vortices moving and staying closer together is suggested by Fig. 7. The vortices become elongated during the initial stage of rotation. By $t=21$ the vortices have rotated and it can be clearly seen that the rotation angle θ is not equal to the inclination of the principal axis of the vortices θ_c. The induced motion includes a component that moves the vortices closer together in a sliding motion. This effect remains in place during the whole of the pairing process and causes the vortices to move together, even when the point vortex model would have the vortices moving apart. If this mechanism is accepted then one possible explanation of the effect of compressibility is apparent—that the change in the vortex elongation affects the pairing process. In particular it would seem that the tendency for vortices to merge would be enhanced by increasing vortex elongation. In this section we investigate this in more detail by conducting vortex dynamics simulations with a vortex model chosen to include simple shape effects.

To model the pairing process we consider a more complex vortex that reflects the motion shown on Fig. 7. The model for the vortices consists of a straight vortex sheet with circulation γ that varies linearly from zero at the ends up to γ_c at the center. Control points are fixed at the quarter and three-quarter positions along the sheet. This pair of coordinates is stored for each vortex allowing the angle of inclination to be found. For an isolated vortex of this kind the rate of precession is about 5% higher than the preces-

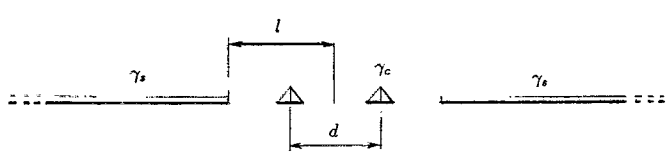

FIG. 8. Sketch of the arrangement of vortex sheets to compute vortex trajectories.

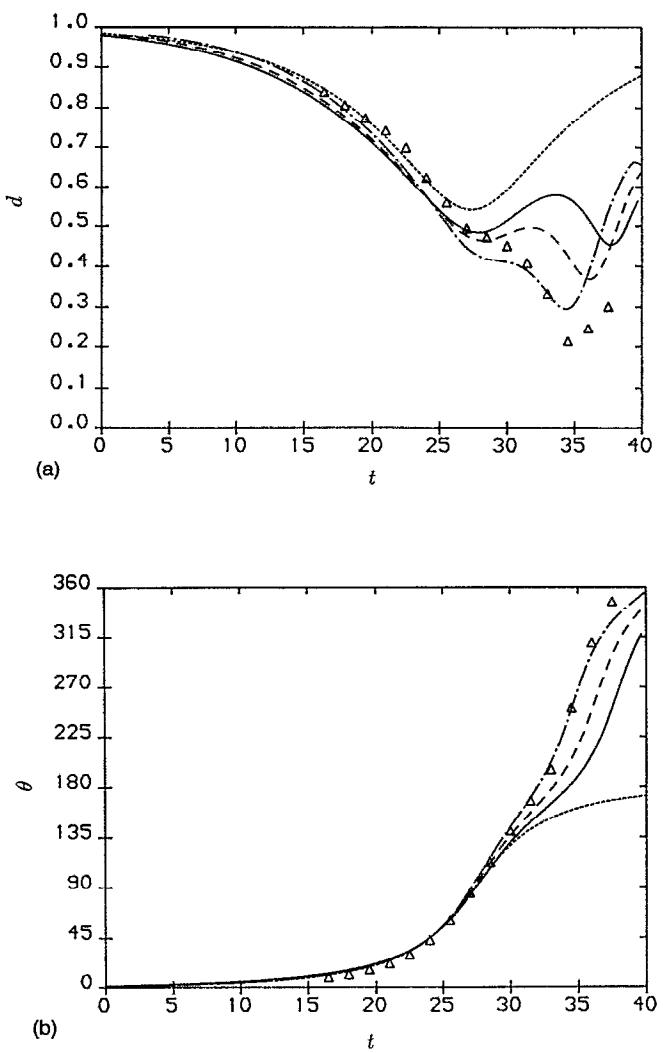

FIG. 9. Vortex simulation of pairing (a) separation of the vortices and (b) rotation of the vortices. Vortex length $c=2$(——), 3(– – –), and 4(– · –). Also shown is the point vortex result (----) and the simulation result for $M_c=0.2$ (symbols).

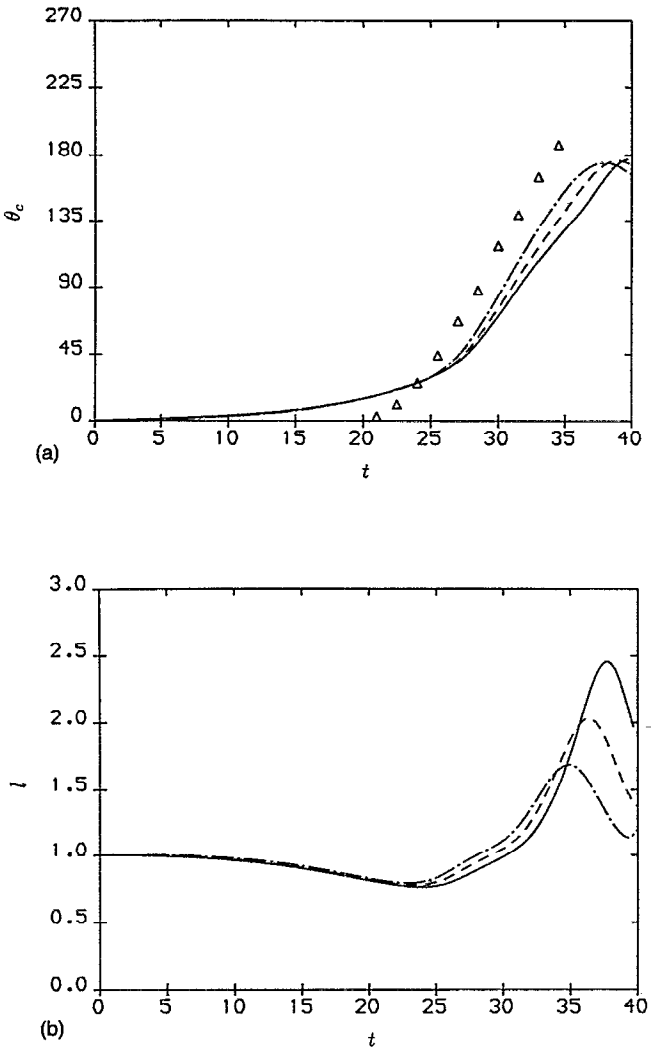

FIG. 10. Vortex simulation of pairing showing core effects (a) rotation of vortex axis and (b) length of the vortex. Vortex length $c=2$(——), 3(– – –), and 4(– · –). Also shown is the point vortex result (----) and the simulation result for $M_c=0.2$ (symbols).

sion rate of an elliptic vortex with uniform vorticity.

We consider an arrangement of two such vortices trapped between two segments of a vortex sheet of strength γ_s, as sketched in Fig. 8. This is a realistic model of the corresponding periodic case. For point vortices the minimum spacing at $\theta=90°$ as a fraction of the initial spacing is 0.541 from this model, as compared to 0.561 for a row of point vortices. For internal shape effects the differences are expected to be even smaller. Numerical computation of the time evolution of the vortices is achieved by summing up the contributions from all the vortex sheets in the flow. The velocities induced can be found by standard panel methods.[6] For the self-induced motion of a single segment, with circulation increasing from zero at one end up to γ_c, and with the control point halfway along the sheet, we have

$$u=0,\qquad v=\gamma_c/2\pi. \tag{4}$$

For the induced motion at some point (x,y) not on the sheet we have

$$u=\frac{\gamma_c}{2\pi s}\left[x\left(\arctan\frac{y}{x-s}-\arctan\frac{y}{x}\right)-\frac{y}{2}\ln\frac{x^2+y^2}{(x-s)^2+y^2}\right],$$
$$v=\frac{\gamma_c}{2\pi s}\left[1-y\left(\arctan\frac{y}{x-s}-\arctan\frac{y}{x}\right)-\frac{x}{2}\ln\frac{x^2+y^2}{(x-s)^2+y^2}\right], \tag{5}$$

where s is the length of the sheet. For the induced motion at some point (x,y) due to a uniform vortex sheet of strength γ_s extending from $-l_\infty$ to $-l$ we have

$$u=\frac{\gamma_s}{2\pi}\left(\arctan\frac{y}{x+l}-\arctan\frac{y}{x+l_\infty}\right),$$
$$v=\frac{\gamma_s}{4\pi}\ln\frac{(x+l)^2+y^2}{(x+l_\infty)^2+y^2}. \tag{6}$$

To get the total velocity q at a control point the velocity contributions from the various elements are summed as follows:

$$q=k(q_1+q_2)+q_3+q_4+q_{s+}+q_{s-}, \tag{7}$$

where q_1 and q_2 combined are the self-induced motion of a vortex, q_3 and q_4 are the elements of the other vortex in the flow, and q_{s+} and q_{s-} are the induced velocities due to the vortex sheet. For a vortex in a strain field one has to distinguish between the rotation of material lines in the vortex and the precession of the vortex itself. Although a vortex may be trapped in a strain field and not precessing, it is clear that fluid elements within the vortex are still rotating, expanding when the element lines up with one principal axis of strain and compressing along the other. Overall the shape of the vortex is fixed, but motion takes place. To reflect this in the model the constant k is introduced which reduces the precession rate of the vortex by a constant factor to reflect the strain field. In the current simulations k is held fixed at approximately the level required to maintain the initial vortex arrangement as a stable state. A refinement to the current model would be to make k depend upon the length s of the vortices, so that it would change during the simulation. An approximation inherent in the model is that, although the vortex can deform along its axis, it cannot become curved in shape. Hence the model will be less accurate late in the pairing process when the two vortices become wrapped around each other.

To represent the pairing process in the mixing layer, using the same normalization as in the previous section, we set $\gamma_s=2$ and the spacing d between the vortices to be 10. The length l shown on Fig. 8 is set by the condition of initial stability of the arrangement. For point vortices we have

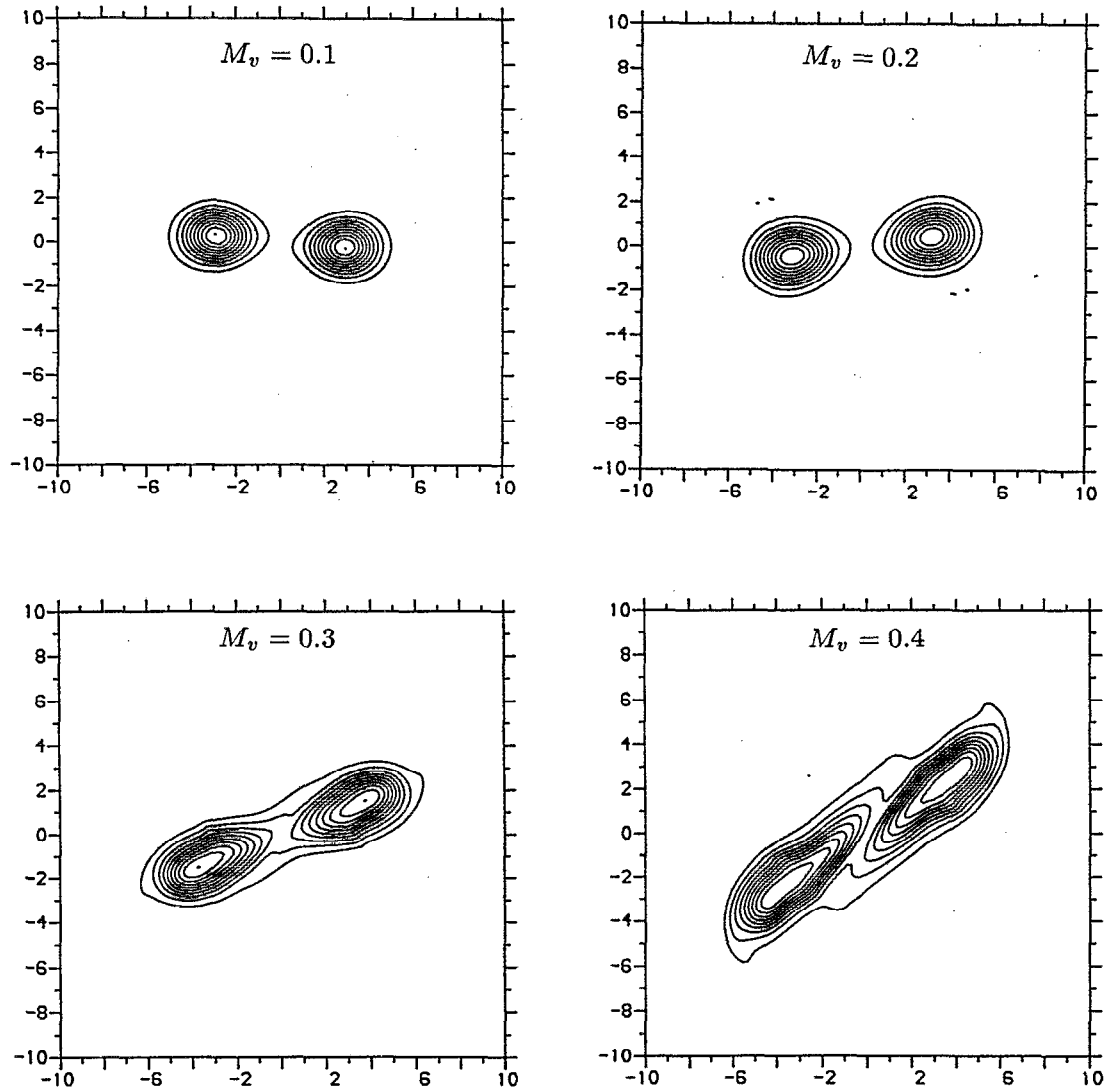

FIG. 11. Contour plots of vorticity for corotating vortex pair at $t=24$ for $M_v=0.1$, 0.2, 0.3, and 0.4. The vortices are rotating clockwise and started out vertically above one another.

$$l=\frac{d(e+1)}{2(e-1)}. \tag{8}$$

For the actual case we use the same value of l, but vary k in (7). The quantity l_∞ is a large number to represent an infinite extent of the constant vortex sheet.

The pairing is triggered by giving a small perturbation to the initial position of the vortices, $\delta x=\delta y=0.1$. The parameter controlling the length of the vortices is c, equal to the distance between the control points on the vortex sheet, or one-half the initial sheet length. Simulations are made for values of c equal to 2, 3, and 4. For these cases the value of k was selected to be 0.043 22, 0.099 80, and 0.185 05, respectively, chosen so that in each case the vortex went though $\theta_c=25°$ at $\theta=45°$. Results for the rotation and separation of the vortices are shown in Fig. 9, and compared with data from the direct simulation at $M_c=0.2$. Since the time axis is somewhat arbitrary, determined by the magnitude of the initial perturbation, it has been ad-

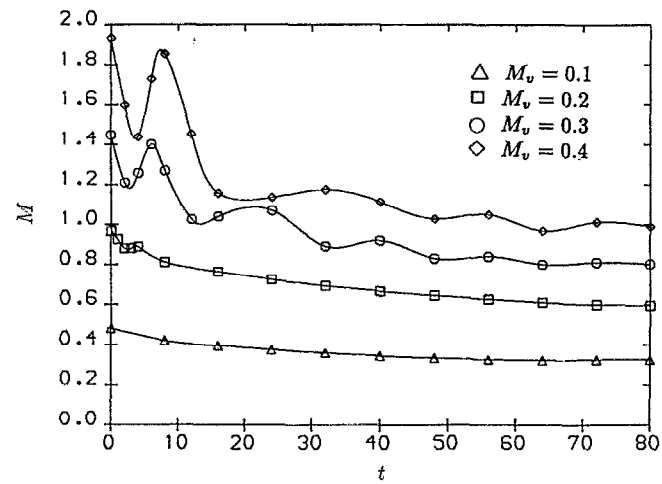

FIG. 12. Variation of the peak Mach number during the simulation of corotating vortices.

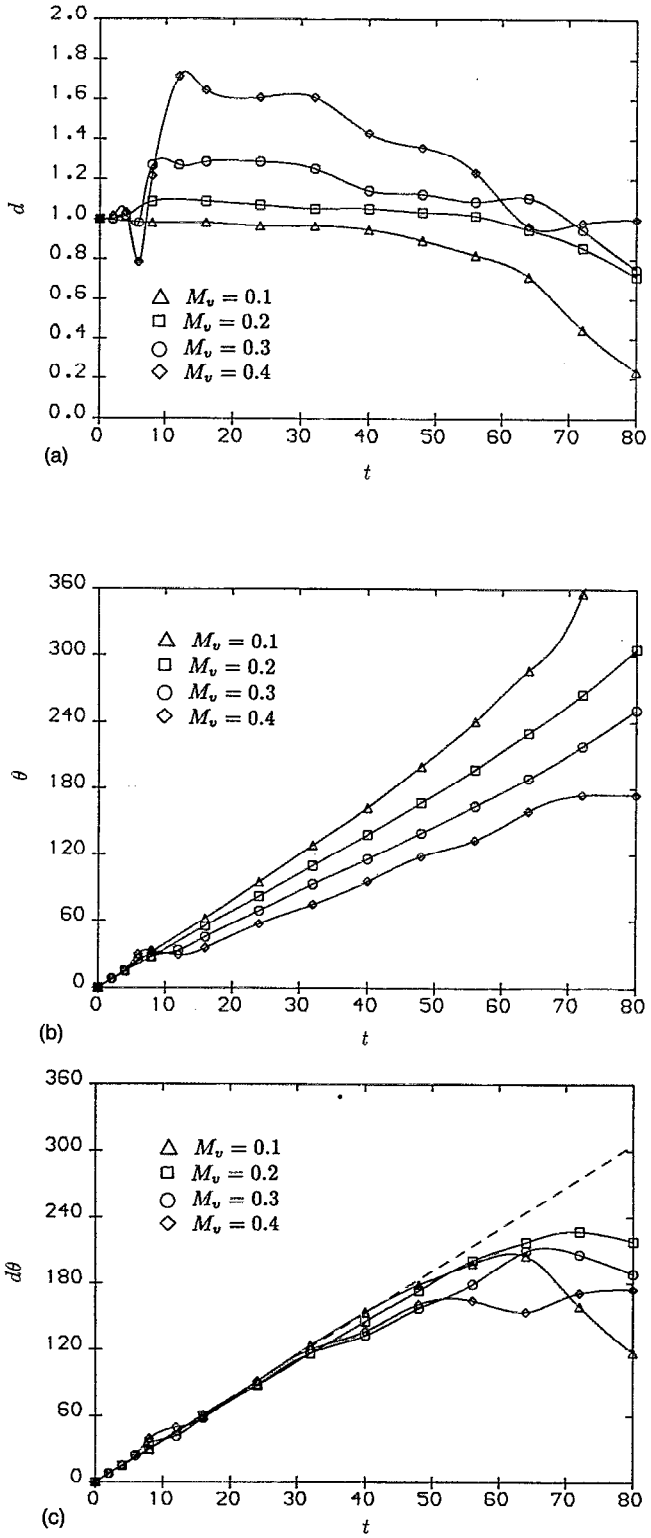

FIG. 13. Graph of the variation in (a) vortex separation, (b) vortex angle, and (c) product of separation and angle for a corotating vortex pair at various Mach numbers.

justed so that the curves pass through $\theta=45°$ at the same time. Also shown is the result for the rotation of two point vortices, which do not get beyond an angle of $\theta=180°$. It can be seen that the rotation angle θ is well predicted for $c=4$ for a complete revolution of the vortices. The spacing shows the correct trend up to $t=28$ for all the choices of c. Behavior beyond $t=28$ is best modeled with $c=4$, which captures the plateau in the variation of spacing for $90°<\theta<180°$ and the renewed reduction in spacing for $\theta>180°$. The effect of increasing c is to reduce the spacing at $\theta=90°$. This was expected as a result of the longer vortex generating more of a sliding motion, bringing the vortices closer together.

Figure 10(a) shows the variation in inclination of the principal axis of the pairing vortices θ_c, compared with simulation data. This measure is well modeled, with the constant value of $\theta_c \approx 180°$ for $180<\theta<360°$ correctly predicted. Variation in the length c of the vortices is shown on Fig. 10(b). This shows that the vortices contract up to $\theta \approx 45°$ and then stretch rapidly up to a maximum length at $\theta \approx 200°$.

Overall this simple "stick" model of vortices captures the main events of pairing quite well. However, taking c as the parameter that models the initial shape of the vortices we see that the effect of changes in c is not the same as the effect of increases in the Mach number. This can be seen by comparing the effect of c shown in Figs. 9 and 10, with the effect of Mach number shown in Fig. 5. With increased M_c we find a more oscillatory behavior of vortex spacing. With increased c the main effect is the reduced spacing at $\theta=90°$ and the stronger reduction in spacing achieved during $180°<\theta<270°$. The conclusion is that the effects of increased Mach number cannot be explained by changes in the initial vortex shape alone.

IV. EVOLUTION OF AN ISOLATED VORTEX PAIR

In this section a corotating pair of vortices with equal circulations is considered. We define a vortex Mach number as follows:

$$M_v=\Gamma/2\pi da, \tag{9}$$

where Γ is the circulation, d is the vortex spacing, and a is the speed of sound.

Direct simulations of corotating vortices were made with a two-dimensional code with the same numerical method applied in each direction (Padé) and with characteristic boundary conditions. The size of the computational domain was 40 in each direction and 150 points were used on a stretched mesh. Vortices were added at (x,y) equal to $(0,3)$ and $(0,-3)$. The vortices consisted of a Gaussian distribution of vorticity leading to the following form for the circumferential velocity:

$$v_\theta=\frac{\Gamma}{2\pi r}\,[1-\exp(-r^2)], \tag{10}$$

where r is the distance from the center of the vortex, and Γ is the circulation. The circulation $\Gamma=2.4\pi$ was chosen, which leads to $M_v=0.2/a$ for the above vortex configuration. Variation in M_v is obtained by changing the sound speed in the simulation. Approximate distributions of the pressure and density perturbations in the vortex are also specified, to reduce the size of the initial transient,

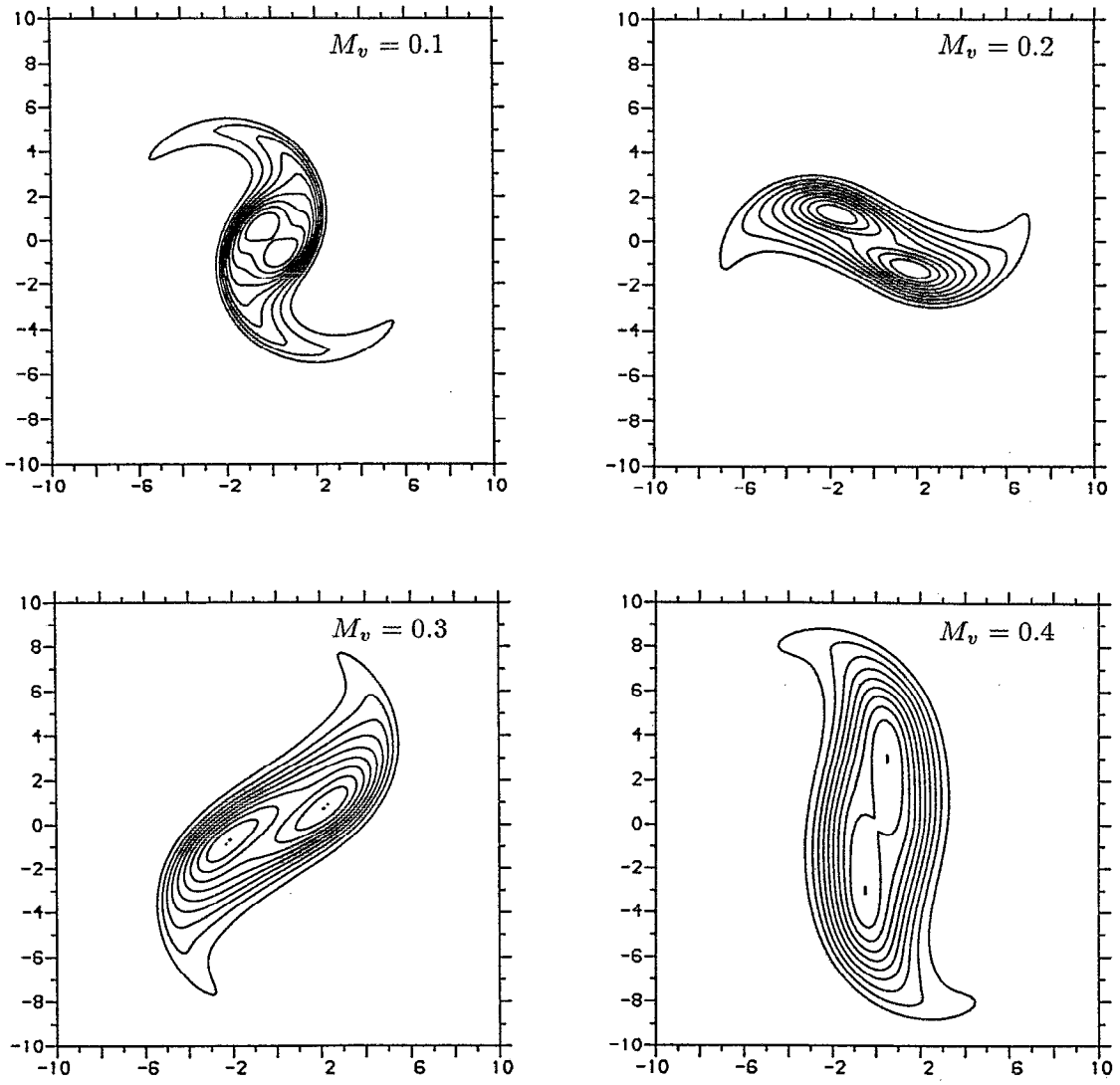

FIG. 14. Contour plots of vorticity for corotating vortex pair at $t=80$ for $M_v=0.1$, 0.2, 0.3, and 0.4.

$$p' = \frac{-0.7\rho a^2}{\gamma(1+r^2)}, \qquad \rho' = \frac{-0.6\rho_\infty}{1+r^2}. \tag{11}$$

The Reynolds number was set to 200.

Simulations were made for corotating vortex pairs with values of M_v equal to 0.1, 0.2, 0.3, and 0.4. Contour plots of vorticity at $t=24$ are shown in Fig. 11 for each Mach number. It can be seen that at the higher Mach numbers the vortices spread out faster and the vorticity at the center of the vortices reduces. This is consistent with theoretical studies[7,8] which show radial velocities for compressible vortices and would tend to smear the vortices out. The maximum value of the local Mach number during the simulations is shown in Fig. 12. There are strong initial transients at the higher Mach numbers. However, in each case the peak Mach number reduces to order unity quite quickly. This supports the sonic eddy model of Breidenthal,[9] which assumes that eddies in a shear layer with Mach numbers above unity do not play a role in entrainment. We find here that vortices with large values of local Mach number spread out quickly so that the actual Mach number reduces.

Figure 13(a) shows the variation of vortex separation with time and Fig. 13(b) shows the vortex angle. The figures show that there is an initial increase in the separation of the vortices, which increases as the Mach number increases. This increase in the separation leads to a decrease in the angular velocity of rotation which explains the slower rotation shown on Fig. 13(b). After the initial transient we find almost no variation of vortex spacing with Mach number, up to $t=32$. On Fig. 13(c) the product of separation and vortex angle is plotted against time and compared with the theoretical result for point vortices with the same circulation. The result is a straight line up until vortex merging and little evidence for a strong effect of Mach number on the induced motions of the vortices. The decrease in the separation observed at longer times is

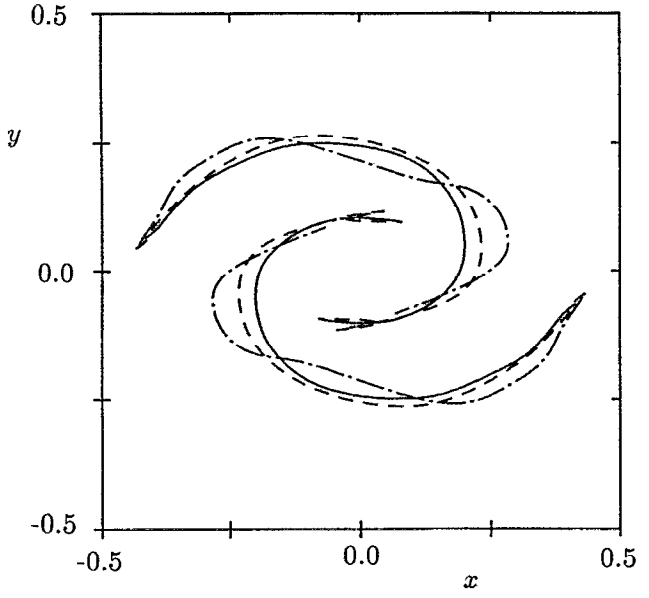

FIG. 15. Vortex trajectories during pairing at convective Mach numbers of 0.2(— —), 0.4(----), and 0.6(– – –). Distances are normalized by the initial vortex spacing.

attributed to merging of the vortex cores, shown in Fig. 14 at time $t=80$.

V. DISCUSSION

To return to the problem of vortex pairing, we can now make some conclusions as to the likely causes of the changes that have taken place. The changes in the details of the pairing can probably not be attributed to either the vortex dynamics of differently shaped vortices, or to any change in the motion of corotating vortices. The most likely explanation is that compressibility effects, similar to those that caused the decrease in the linear instability of the mixing layer, continue to play a role in the vortex pairing process. One feature of the linear instability is that it produces more elongated vortices at higher Mach numbers.[2,10] The subharmonic wave that is associated with the pairing might also be assumed to produce an elongated region of rotation, initially containing the two vortices from the roll-up of the fundamental mode of instability. If the paths of these vortices become more elongated, then during the phase of rotation $90°<\theta<180°$ and $270°<\theta<360°$ the vortices would tend to move apart and during the stages $0°<\theta<90°$ and $180°<\theta<270°$ the vortices would tend to move together. In fact this is borne out by the variation in separation during the pairing process [Fig. 5(a)], which follows a more oscillatory path as the Mach number increases. The changes are shown in Fig. 15, where the actual vortex trajectories are plotted for the three different Mach numbers of the direct simulations.

VI. CONCLUSIONS

An investigation has been made of the effects of compressibility on vortex pairing and isolated vortex pairs. Direct numerical simulations were used to extract data for the position and evolution of the vortices and to pinpoint the trends due to increasing Mach number. Vortex dynamics simulations, based on a vortex sheet model, were shown to do a good job of predicting the motion and orientation of the pairing vortices at low Mach number. However, changing the shape of the vortices in the model did not lead to the same effects as compressibility and so the initial shape of the vortices in the mixing layer was ruled out as the main cause of the compressibility effects. Direct simulations of simple corotating vortices showed that a change in Mach number led to only small changes in the expected rate of rotation of the vortices as a function of vortex separation. Strong core effects were, however, observed at the higher Mach numbers considered. Elongated vortex trajectories were found during pairing, indicating a continuation of the phenomena associated with the nonlinear evolution of the primary instability.

ACKNOWLEDGMENT

This work was supported by a grant from the Nuffield Foundation.

[1] D. W. Moore, "The effect of compressibility on the speed of propagation of a vortex ring," Proc. R. Soc. London Ser. A **397**, 87 (1985).
[2] N. D. Sandham and W. C. Reynolds, "A numerical investigation of the compressible mixing layer," Report TF-45, Department of Mechanical Engineering, Stanford University, Stanford, California, 1989.
[3] N. D. Sandham and W. C. Reynolds, "Three-dimensional simulations of large eddies in the compressible mixing layer," J. Fluid Mech. **244**, 133 (1991).
[4] N. T. Clemens and M. G. Mungal, "Two- and three-dimensional effects in the supersonic mixing layer," AIAA J. **30**, 973 (1992).
[5] S. A. Ragab and J. L. Wu, "Linear subharmonic instabilities of periodic compressible mixing layers," AIAA Paper No. 89-0039, 1989.
[6] J. Katz and A. Plotkin, *Low-Speed Aerodynamics* (McGraw-Hill, New York, 1991).
[7] T. Colonius, S. Lele, and P. Moin, "The free compressible viscous vortex," J. Fluid Mech. **230**, 45 (1991).
[8] E. W. Mayer and K. G. Powell, "Similarity solutions for viscous vortex cores," J. Fluid Mech. **238**, 487 (1992).
[9] R. Breidenthal, "The sonic eddy—a model for compressible turbulence," AIAA J. **30**, 101 (1992).
[10] N. D. Sandham and W. C. Reynolds, "Compressible mixing layer: Linear theory and direct simulation," AIAA J. **28**, 618 (1990).